ELSEVIER
International Journal of Heat and Fluid Flow 21 (2000) 112–121
International Journal of
HEAT AND FLUID FLOW
www.elsevier.com/locate/ijhff

Lattice Boltzmann simulation of multiphase fluid flows through the total variation diminishing with artificial compression scheme

Shulong Teng *, Yu Chen, Hirotada Ohashi

Department of Quantum Engineering and Systems Science, Faculty of Engineering, The University of Tokyo, 7-3-1 Hongo, Bunkyo-ku, 113-8656 Tokyo, Japan

Received 7 May 1999; accepted 17 August 1999

Abstract

The total variation diminishing with artificial compression (TVD/AC) scheme is applied to the lattice Boltzmann multiphase model in order to introduce a new technique to solve the traditional lattice Boltzmann equation. The TVD/AC scheme gives a much higher resolution than the well-known TVD scheme to the interface in the simulation of multiphase flows. Numerical simulations also show that the new simulator is helpful in stabilizing the computation in the runs of high-density ratios. Numerical results for the coexistence curve and verification of the Laplace law both in two and three spatial dimensions are presented. The detailed dynamical behaviors of the interface over a wide range of density ratios such as the variation of interface thickness and profiles of density, the balance of pressure and interfacial stress, the distribution of spurious velocities and so on are studied. Phase separation in two- and three-dimensional systems is also demonstrated numerically. © 2000 Elsevier Science Inc. All rights reserved.

Keywords: Multiphase flow; Lattice Boltzmann method; TVD/AC scheme; Interface; Numerical simulation

Notation

c	microscopic particle velocity
f	distribution function
F	force experienced by molecules
l	length
L	anti-diffusion term
M	minmod function
p	pressure
Q	function helpful to eliminate the so-called entropy violation
R	radius
Re	Reynolds number
S	sign function
t	time
T	temperature
u	velocity
We	Weber number
x	Cartesian coordinate
Greeks	
α	surface tension coefficient
$\varepsilon_h^{\mathrm{d}}$	discretization error
κ	dimensionless collision frequency
λ	constant parameter that controls the strength of the surface tension effect
ν	kinematic viscosity
ρ	density
$\sigma^{(1)}$	interfacial stress tensor
$\sigma^{(\nu)}$	viscous stress tensor
ξ	non-dimensional number
Subscripts	
c	critical
i	index
r	reference
α, β, γ	spatial directions in Cartesian coordinates
Superscript	
n	time step

1. Introduction

Multiphase flows are difficult to study both from the physical and computational points of view due to the complexity of the physics especially involved in the interfacial dynamics. In the past few years, the lattice Boltzmann method (LBM) (Benzi et al., 1992; Qian et al., 1995; Chen and Doolen, 1998) has been an attractive alternative to solve fluid flow, taking advantage of its parallel nature, simple algorithm and easy to implement complicated boundary conditions. It also provides a method to model multiphase flows at the microscopic scale through incorporating the non-local interaction of particles and meanwhile can fully recover the Navier–Stokes equations at the macroscopic scale.

---

* Corresponding author.
E-mail address: teng@crimson.q.t.u-tokyo.ac.jp (S. Teng).

PII: S0142-727X(99)00068-5

In this paper, we first briefly review some recent developments in this field and then point out the common problems in the numerical schemes. Finally we introduce a technique to solve them and show the improved results.

The initial LBM multiphase model (Gunstensen et al., 1991) was based on the immiscible lattice gas automata (ILGA) model (Rothman and Keller, 1988) and aimed at eliminating some unphysical effects in the LGA model (Chen et al., 1991) with the advantages of the lattice Boltzmann approach. Grunau et al. (1993) later developed a model by using a single-time relaxation procedure and allowed variations of density and viscosity. But the drawback of these models is that the system relaxes to an equilibrium state that cannot be described thermodynamically. Shan and Chen (1993, 1994) and Shan and Doolen (1995) made some improvements on solving this problem through the introduction of an interparticle potential to their model. Swift et al. (1995, 1996) proposed an LBM multiphase model in which the collision rules were chosen such that the equilibrium state corresponds to an input free energy, which is similar in spirit to the Cahn–Hillard theory of phase transitions. Chen et al. (1998), through the comparison with a macroscopic two-phase fluid flow model suggested by Nadiga and Zaleski (1996), derived a lattice Boltzmann equation from the continuous Boltzmann BGK equation with an external force term. In this model, phase separation and interface formation are naturally driven by an intermolecular interaction. From the kinetic theory, Zou and He (1999) directly derived almost the same model of Chen and provided this model with a solid physical foundation. This is the reason why we chose this model in our study. Details of the model will be introduced in Section 2.

Through the investigation of previous studies, we found that the algorithms of solving these models were all restricted in the traditional LBE scheme basically due to its simplicity. But this scheme has two main obvious drawbacks: (1) it is difficult to apply non-uniform grids in the scheme; (2) the scheme intends to be unstable when density ratios are high in the simulations of multiphase flows. These two drawbacks set an obstacle to the ability of the method to handle complex geometries such as those commonly encountered in most CFD engineering applications. Especially the second drawback prevents us from calculating multiphase flows over a wide range of density ratios. To the best of our knowledge, multiphase flows with the LBM model in which density ratio is raised more than 20 have not been studied yet. We hope this study could help in filling this gap by solving the lattice Boltzmann equation with a more sophisticated scheme.

By borrowing some standard ideas from the finite-difference method, the original LBE can be extended in such a way as to handle Cartesian arbitrary geometries. Then the space and time steps need not be treated as unit ones (like those in the standard LBE), so that we can choose any space and time steps including non-uniform grids and different Courant numbers. Based on the original TVD scheme, Jin (1993) developed a TVD/AC scheme which pays special attention to the contact discontinuity in numerical simulations. It gives a much higher resolution than the TVD scheme to the interface in the simulations of multiphase flows. Details of this scheme are given in Section 3. Numerical simulation results and conclusions are presented in Section 4 and 5, respectively.

2. The lattice Boltzmann multiphase model

The dimensionless Boltzmann equation with the Bhatnagar–Gross–Krook (BGK) approximated collision term is as follows:

$$\frac{\partial f}{\partial t} + c_\alpha \frac{\partial f}{\partial x_\alpha} + F_\alpha \frac{\partial f}{\partial c_\alpha} = \frac{\kappa}{\xi}(f^{\mathrm{eq}} - f), \tag{2.1}$$

where f is the single-particle distribution function for a one-chemical-component system, c the microscopic particle velocity, F the force experienced by molecules, κ the dimensionless collision frequency, ξ a non-dimensional number which is proportional to the Knudsen number (ratio of the mean free path to the macroscopic characteristic length). By discretizing the velocity space with Gauss–Hermite quadrature (Chen et al., 1998), the discrete Boltzmann equation for multiphase flows can be derived as

$$\frac{\partial f_i}{\partial t} + c_{i\alpha} \frac{\partial f_i}{\partial x_\alpha} = \frac{\kappa}{\xi}(f_i^{\mathrm{eq}} - f_i) + 3F_\alpha (c_{i\alpha} - u_\alpha) f_i^{\mathrm{eq}}. \tag{2.2}$$

Macroscopic fluid density ρ, velocity $\vec{u}$ and temperature T can be calculated as the velocity moments of the discrete distribution function

$$\rho = \sum_i f_i, \tag{2.3}$$

$$\rho\vec{u} = \sum_i f_i \vec{c}_i, \tag{2.4}$$

$$3\rho RT = \sum_i f_i (\vec{c}_i - \vec{u})^2. \tag{2.5}$$

Through the Chapman–Enskog expansion (Frisch et al., 1987) to ξ^2order accuracy and a multi-scale analysis, the macroscopic equations for mass and momentum are obtained as follows:

$$\frac{\partial \rho}{\partial t} + \frac{\partial}{\partial x_\alpha}(\rho u_\alpha) = 0, \tag{2.6}$$

$$\frac{\partial}{\partial t}(\rho u_\alpha) + \frac{\partial}{\partial x_\beta}(\rho u_\alpha u_\beta) = -\frac{\partial}{\partial x_\alpha}\left(\frac{\rho}{3}\right) + \frac{\partial}{\partial x_\beta}\left[\frac{\rho\xi}{3\kappa}\left(\frac{\partial u_\alpha}{\partial x_\beta} + \frac{\partial u_\beta}{\partial x_\alpha}\right)\right] + \rho F_\alpha. \tag{2.7}$$

Still missing from the approach is a macroscopic differential equation describing energy conservation. Although such an equation has been included in a lattice Boltzmann scheme for an ideal gas (Alexander et al., 1993), it is far from obvious how to treat potential energy correctly in the multiphase model. Therefore simulations in this paper are assumed to be isothermal. Parameters appearing in the discrete Boltzmann equation are set according to the macroscopic flow through the following relationship:

$$\frac{\kappa}{\xi} = \frac{Re_{\mathrm{r}}}{3}, \tag{2.8}$$

$$F_\alpha = \left(\frac{1}{3\rho} - \frac{3}{\rho(3-\rho)^2} + \frac{3}{4T}\right)\frac{\partial \rho}{\partial x_\alpha} + \frac{1}{We_{\mathrm{r}}}\nabla^2 \frac{\partial \rho}{\partial x_\alpha}, \tag{2.9}$$

Re_{r} and We_{r} are reference Reynolds and Weber numbers, dimensionless parameters which characterize the flow field. With such a relationship, the macroscopic equation will be the same with the model proposed by Nadiga and Zaleski (1996) in which a stress tensor $\sigma^{(1)}$ derived from the van der Waals–Cahn–Hilliard free energy is directly added to the Navier–Stokes equations:

$$\frac{\partial \rho}{\partial t} + \frac{\partial}{\partial x_\alpha}(\rho u_\alpha) = 0, \tag{2.10}$$

$$\frac{\partial}{\partial t}(\rho u_\alpha) + \frac{\partial}{\partial x_\beta}(\rho u_\alpha u_\beta) = -\frac{\partial}{\partial x_\alpha}p(\rho) + \frac{\partial}{\partial x_\beta}\sigma_{\alpha\beta}^{(v)} + \frac{\partial}{\partial x_\beta}\sigma_{\alpha\beta}^{(1)}, \tag{2.11}$$

where $\sigma^{(v)}$ is the ordinary viscous stress tensor. For the dimensionless definition, $\sigma^{(v)}$ is expressed as

$$\sigma^{(v)}_{\alpha\beta} = \frac{\rho}{Re_{\mathrm{r}}}\left(\frac{\partial u_\alpha}{\partial x_\beta} + \frac{\partial u_\beta}{\partial x_\alpha} - \frac{2}{3}\frac{\partial u_\gamma}{\partial x_\gamma}\delta_{\alpha\beta}\right). \tag{2.12}$$

The interfacial stress tensor $\sigma^{(1)}$ depends on the density gradient which is defined as

$$\sigma^{(1)}_{\alpha\beta} = \frac{1}{We_{\mathrm{r}}}\left[\left(\frac{1}{2}|\nabla\rho|^2 + \rho\nabla^2\rho\right)\delta_{\alpha\beta} - \frac{\partial\rho}{\partial x_\alpha}\frac{\partial\rho}{\partial x_\beta}\right]. \tag{2.13}$$

The reference Reynolds number and Weber number are defined as

$$Re_{\mathrm{r}} = \frac{c_{\mathrm{r}} l_{\mathrm{r}}}{v}, \quad We_{\mathrm{r}} = \frac{c_{\mathrm{r}}^2 l_{\mathrm{r}}^2}{\lambda\rho_{\mathrm{r}}},$$

respectively. Here $c_{\mathrm{r}}, l_{\mathrm{r}}, \rho_{\mathrm{r}}$ are the reference velocity, length and density. Parameter v is the kinematic viscosity, λ a constant parameter that controls the strength of the surface tension effect. From the definition of interfacial stress tensor $\sigma^{(1)}$, the surface tension coefficient α at a planar interface normal to the y direction can be derived as

$$\alpha = \frac{1}{We_{\mathrm{r}}}\int_{-\infty}^{+\infty}\left(\frac{\mathrm{d}\rho}{\mathrm{d}y}\right)^2 \mathrm{d}y. \tag{2.14}$$

A number of equations of state, such as two-constant equations of van der Waals, Dieterici, Berthelot and so on (Hirschfelder et al., 1964) can be served in the simulations. The dimensionless van der Waals equation we used in this model is expressed as

$$P = \frac{\rho}{3-\rho} - \frac{3\rho^2}{8T}. \tag{2.15}$$

Such an equation of state allows for the existence of two phases of different densities, a low density phase that we call the gas-phase and a high density phase that we call the liquid-phase.

Reference quantities for normalization are chosen as follows

$$\rho_{\mathrm{r}} = \rho_{\mathrm{c}}, \quad T_{\mathrm{r}} = T_{\mathrm{c}}, \quad \upsilon_{\mathrm{r}} = \sqrt{3RT}, \quad t_{\mathrm{r}} = l_{\mathrm{r}}/\upsilon_{\mathrm{r}},$$

where $\rho_{\mathrm{c}}, T_{\mathrm{c}}, t_{\mathrm{r}}$ are critical density, critical temperature and reference time, respectively.

From the viewpoint of intermolecular interaction, Zou and He (1999) proposed the same Boltzmann model for multiphase flows. They considered two important facts in deriving the process. First, the collision term needs to be modified because the particle size becomes comparable to the free path of molecules for a dense gas or a liquid. Second, the intermolecular attraction may become important especially for fluids involved in phase separations and transitions such as multiphase flows. Besides, the method is in fact a 'discrete velocity Boltzmann model', but according to the background of the model derivation from the continuous Boltzmann BGK equation, customarily we call it the lattice Boltzmann model.

As for the discrete velocity set $\{\vec{c}_i\}$ and definiton for f^{eq}, we employ the D2Q9 model (Qian et al., 1992) in two-dimensional and the D3Q15 model in three-dimensional systems.

3. The TVD/AC scheme

TVD/AC is TVD with artificial compression scheme. It is based on the TVD scheme and an anti-diffusion term is added to improve the resolution of the contact discontinuity. The TVD scheme is effective for solving the problem of shock wave propagation. In it, physical compression compensates for the numerical diffusion across a shock front. However, numerical diffusion still exists when the characteristics associated with a discontinuous wave are not in a shock-line fashion. The contact discontinuity in the multiphase flow is not compressive in this sense. Therefore, if the TVD scheme is applied to solve this kind of problem, the fluid interface is diffusive. But TVD/AC is instead a very efficient method with enhanced resolution and accuracy for the multiphase flow problem. It does not spoil the physics of the problem but only decreases the numerical diffusion with an anti-diffusion term.

For simplicity, a scalar linear wave equation is considered as the example to introduce the TVD/AC scheme

$$\frac{\partial f}{\partial t} + a\frac{\partial f}{\partial x} = 0, \tag{3.1}$$

where a is a constant. Here we first briefly review the TVD scheme (Harten, 1983) as it is the basis of the TVD/AC scheme. The TVD scheme advances the solution of Eq. (3.1) at time level $n+1$ and grid point 'i' via the equation

$$f_i^{n+1} = f_i^n - \lambda\left(F^n_{i+1/2} - F^n_{i-1/2}\right), \tag{3.2}$$

where $F^n_{i+1/2}$ is the numerically calculated flux,

$$F^n_{i+1/2} = \tfrac{1}{2}\left(af_i^n + af_{i+1}^n + g_i^n + g_{i+1}^n - Q(a+\gamma^n_{i+1/2})\Delta^n_{i+1/2}\right), \tag{3.3}$$

$$g_i^n = M\left(\tilde{g}^n_{i-1/2}, \tilde{g}^n_{i+1/2}\right), \tag{3.4}$$

$$\tilde{g}^n_{i+1/2} = \tfrac{1}{2}\left(Q(a) - \lambda a^2\right)\Delta^n_{i+1/2}, \tag{3.5}$$

$$\Delta^n_{i+1/2} = f^n_{i+1} - f^n_i, \tag{3.6}$$

and M is the minmod function,

$$M(x_1, x_2, \ldots, x_n) = \begin{cases} \operatorname{sign}(x_1)\min(|x_1|, |x_2|, \ldots, |x_n|), & \text{all } x_i \text{ have same sign,} \\ 0 & \text{otherwise.} \end{cases} \tag{3.7}$$

$Q(x)$ is a function helpful to eliminate the so-called entropy violation,

$$Q(x) = \begin{cases} (x^2/(4\varepsilon)) + \varepsilon & \text{for } |x| < 2\varepsilon, \\ |x| & \text{for } |x| \geqslant 2\varepsilon, \end{cases} \tag{3.8}$$

where ε is a positive constant generally taken to be between 0.1 and 0.5. In the following numerical simulations, we choose ε to be 0.2.

The definition of γ is

$$\gamma^n_{i+1/2} = \begin{cases} \left(g^n_{i+1} - g^n_i\right)/\Delta^n_{i+1/2} & \Delta^n_{i+1/2} \neq 0, \\ 0, & \Delta^n_{i+1/2} = 0. \end{cases} \tag{3.9}$$

For TVD/AC scheme, an anti-diffusion term $L(f)$ is added to Eq. (3.1) to improve the resolution of the contact discontinuity

$$\frac{\partial f}{\partial t} + \frac{\partial}{\partial x}(af + L(f)) = 0. \tag{3.10}$$

Then we have a new numerical flux

$$\begin{aligned} F^n_{i+1/2} = \frac{1}{2}(&af_i^n + af_{i+1}^n + L_i^n + L_{i+1}^n + g_i^n + g_{i+1}^n \\ &- Q(a + \upsilon^{LM}_{i+1/2} + \gamma^n_{i+1/2})\Delta^n_{i+1/2}), \end{aligned} \tag{3.11}$$

where

$$\upsilon^{LM}_{i+1/2} = \begin{cases} (L^n_{i+1} - L^n_i)/\Delta^n_{i+1/2}, & \Delta^n_{i+1/2} \neq 0, \\ 0, & \Delta^n_{i+1/2} = 0 \end{cases} \tag{3.12}$$

and the definition of $\gamma^n_{i+1/2}$ is the same as Eq. (3.9),

$$\tilde{g}^n_{i+1/2} = \tfrac{1}{2}\left(Q\left(a+v^{LM}_{i+1/2}\right) - \lambda\left(a+v^{LM}_{i+1/2}\right)^2\right)\Delta^n_{i+1/2}. \tag{3.13}$$

To preserve all properties of the TVD scheme, $L^n_i$is taken to be of the form

$$L^n_i = S\cdot\max\left(0, M\left(\eta L^n_{i-1/2}, L^n_{i+1/2}\right)\cdot S, M\left(L^n_{i-1/2}, \eta L^n_{i+1/2}\right)\cdot S\right). \tag{3.14}$$

Here $S = \mathrm{sign}(L^n_{i+1/2})$ and

$$L^n_{i+1/2} = \tfrac{1}{2}\left(Q(a)-\lambda a^2\right)\left(\Delta^n_{i+1/2} - M\left(\Delta^n_{i-1/2}, \Delta^n_{i+1/2}, \Delta^n_{i+3/2}\right)\right). \tag{3.15}$$

The purpose of introducing a parameter η is to keep L^n_i to be of $O(\Delta x^2)$ in an interval for which the solution is smooth. We take η to have the form

$$\eta = 2\left|\frac{\left|\Delta^n_{i+1/2}\right|^\beta - \left|\Delta^n_{i-1/2}\right|^\beta}{\left|\Delta^n_{i+1/2}\right|^\beta + \left|\Delta^n_{i-1/2}\right|^\beta}\right|, \quad \beta = 2.5. \tag{3.16}$$

When $\eta \approx 0$ (this occurs when $\Delta^n_{i-1/2} \approx \Delta^n_{i+1/2}$), the scheme is the same as the TVD scheme. It can be proved that the new scheme does not change the order of accuracy of the TVD scheme. On the other hand, at the hill and cliff regions of discontinuity where the difference between $|\Delta^n_{i-1/2}|$ and $|\Delta^n_{i+1/2}|$ is large, the effect of finite η (therefore finite L^n_i) will contribute to flux like a source term. The extent to which η affects the steepening of the discontinuity can be adjusted by changing the value of β. In our simulations we choose β to be 2.5.

A Riemann problem for Eq. (3.1) is used to make a simple comparision of different schemes

$$f(x,0) = \begin{cases} f_L & x < 0, \\ f_R & x > 0. \end{cases}$$

Fig 1(a–c) show the results obtained by the MacCormack, TVD and TVD/AC schemes. From Fig. 1(a) we can see that numerical oscilations occurred in the result of the MacCormack scheme when the ratio of f_L to f_R equals 10. In fact, the same problem exists in the traditional LBE scheme and this is one reason we employ the TVD/AC scheme in this paper. In Fig. 1(b) the width of the contact discontinuity in the TVD scheme is about 7–8 mesh blocks while it is only 3–4 blocks for the TVD/AC scheme in Fig. 1(c). Fig. 1(d) shows that even when the ratio of f_L to f_R equals 10^5, the TVD/AC scheme could still keep the sharpening in the contact discontinuity.

It is straightforward to apply the TVD/AC scheme to the discrete Boltzmann equation (2.2) because of its linear streaming term in which all discrete speeds are of the same magnitude $|\vec{c}_i| = c$. The right-hand part of (2.2) is treated as a

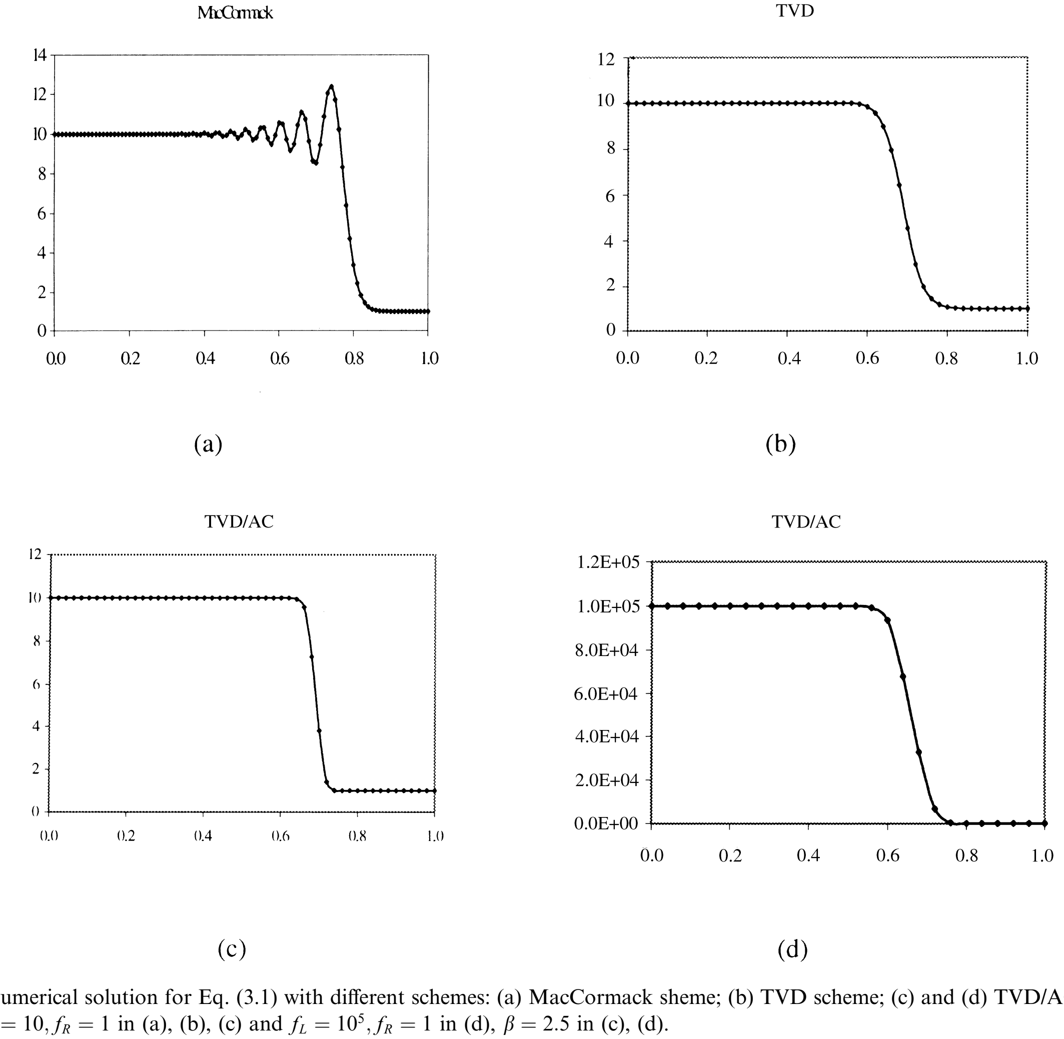

(a) (b)

(c) (d)

Fig. 1. The numerical solution for Eq. (3.1) with different schemes: (a) MacCormack sheme; (b) TVD scheme; (c) and (d) TVD/AC scheme. Initial condition: $f_L = 10, f_R = 1$ in (a), (b), (c) and $f_L = 10^5, f_R = 1$ in (d), $\beta = 2.5$ in (c), (d).

source term and the second order Runge–Kutta method (Press et al., 1989) is used for time integration so that both in space and time numerical solutions are second order accurate.

4. Numerical simulations

4.1. Verification of the model and the scheme

4.1.1. The densities of the coexisting phases at different temperatures

First, densities of the coexisting phases at different temperatures are verified. According to a thermodynamic calculation in which the Gibbs free energies of the two phases at the given temperature are equated, which is also called Maxwell equal area construction (Rowlinson and Widom, 1982), the theoretical densities of the two coexisting phases at different temperatures can be calculated and the results are shown as the curve in Fig. 2(a). The points in Fig. 2(a) are obtained by equilibrating a flat interface between the liquid and gas phases for different temperatures. The initial density distribution is set up so that the density in half of the domain is higher than that in the other half. The size of the system is 0.5 × 1.0 with a 50 × 100 computational grid. The Courant number is 0.2 and therefore the time increment is 0.002 since the maximum discrete velocity is a unit in the model. Except for special declarations, Courant numbers in all after simulations are also taken as 0.2. Doubly periodic condition is imposed and it takes about 100 dimen-

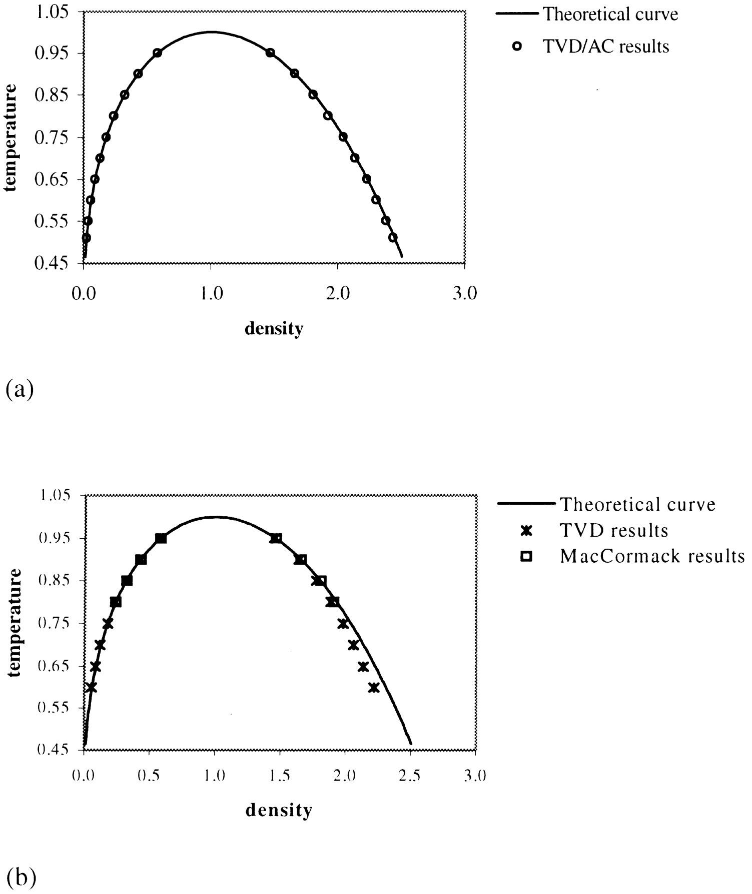

(a)

(b)

Fig. 2. The densities of the coexisting phases at different temperatures calculated with different schemes.

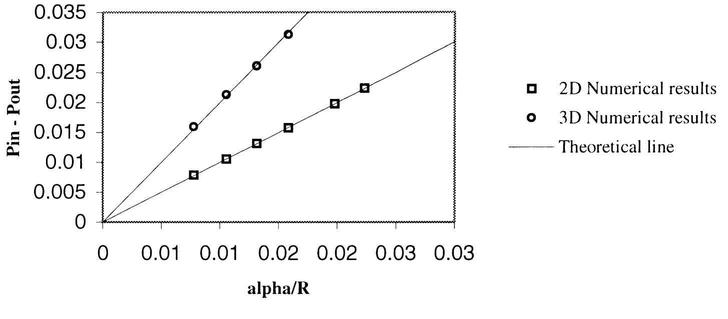

Fig. 3. Verification of Laplace law. On the x-axis α/R is plotted. On the y-axis is the numerically measured pressure difference between the inside and the outside of the drop.

sionless time for the system to reach equilibrium. From the figure we can see that the numerical results agree with the theoretical curve very well over a wide range of density ratios. When the dimensionless temperature equals 0.51, the density ratio reaches 100 and numerical stability is still well kept. We also performed the same simulations with MacCormack and TVD schemes and the results are shown in Fig. 2(b). The lowest temperature is 0.8 and 0.6, respectively. For even lower temperatures, the simulation becomes numerically unstable. Fig. 2(b) also shows that the TVD scheme is not as accurate as the TVD/AC scheme in the runs of large density ratios.

4.1.2. Laplace law

According to the Laplace law (Rowlinson and Widom, 1982), the tension in the surface will make the bubble collapse unless the pressure inside exceeds that outside by, say, Δp. The work of a virtual increase in R vanishes at equilibrium, so $\delta p \mathrm{d}V$ equals $\alpha \mathrm{d}A$, where $\mathrm{d}V$, α and $\mathrm{d}A$ are the increases in volume, the surface tension and area of the sphere. In a d-dimensional space $\mathrm{d}V/\mathrm{d}A = (d-1)^{-1}R$, and so, for $d = 2$

$$\Delta p = \frac{\alpha}{R},$$

for $d = 3$,

$$\Delta p = \frac{2\alpha}{R}.$$

The initial condition of simulations here is to let a droplet be suspended in the gaseous phase. The pressure difference across the liquid–vapor interface is calculated when dimensionless time equals 25, which is necessary for equilibration. When the droplet get to equilibrium, it is found that its shape does not change any longer and it also does not depart from a circle. The pressure inside the droplet is measured by averaging the pressure at all sites inside a sphere of radius about $0.7R$, while the outside pressure is measured by averaging the pressure at all sites having a distance to the center of the droplet larger than $1.3R$. The non-dimesional surface tension α is calculated by Eq. (2.14). Tests at the condition of $T = 0.8$ are carried out both in two and three dimensions. When $R = 0.1$, runs of $We_r = 20\,000$ and $40\,000$ corresponding to surface tension $\alpha = 2.24 \times 10^{-3}$ and 1.58×10^{-3}, respectively are calculated in two-dimensional space. When $\alpha = 1.58 \times 10^{-3}$, runs of different R are also calculated in two- and three-dimensional spaces. The size of the system in two dimensions is 0.5×0.5 with a 100×100 computational grid and $0.4 \times 0.4 \times 0.4$ with a $80 \times 80 \times 80$ computational grid in three dimensions. Numerical results are all shown in Fig. 3. The satisfactory agreement between the simulation and the analytical results verifies the consistency in the modeling of the surface tension and also demonstrates the successful employment of the TVD/AC scheme in lattice Boltzmann equation both in two and three dimensions.

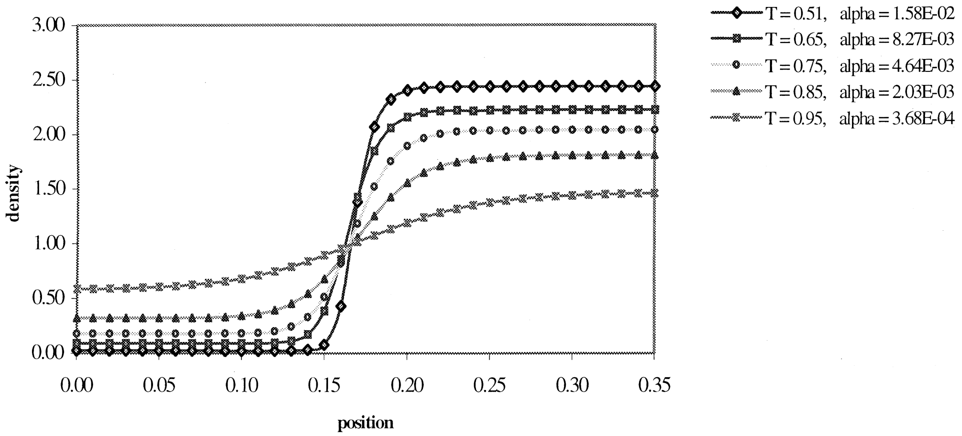

Fig. 4. Equilibrium density profiles normal to a flat interface at different temperature with $We_r = 10\,000$ when $t = 100$ (α is dimensionless surface tension coefficient).

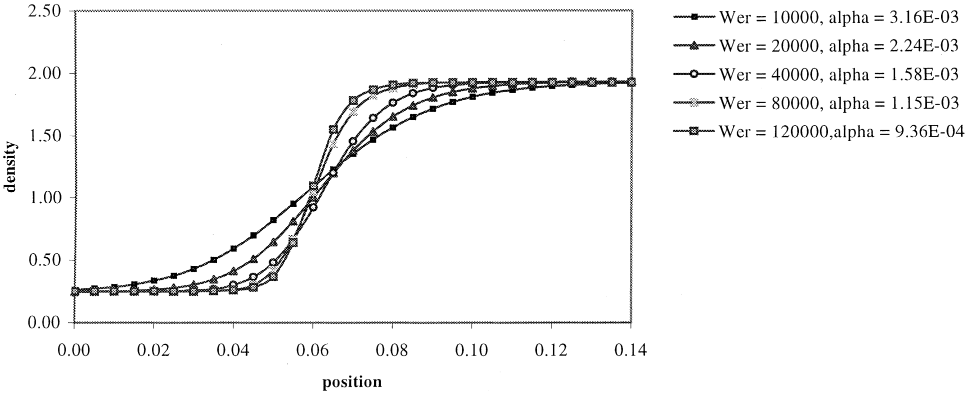

Fig. 5. Equilibrium density profiles normal to a flat interface with different Weber numbers at $T = 0.8$, $t = 100$.

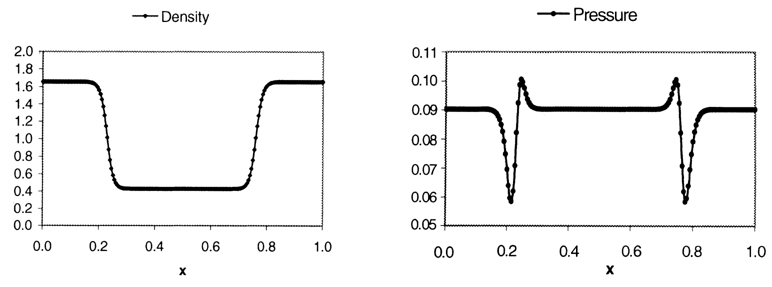

(a) Density profile.

(b) Pressure profile.

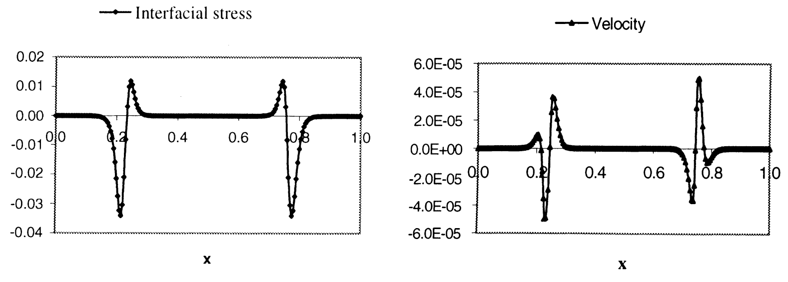

(c) Interfacial stress profile.

(d) Velocity distribution

Fig. 6. Equilibrium parameters profile normal to a flat interface: (a) density; (b) pressure; (c) interfacial stress; (d) spurious velocity.

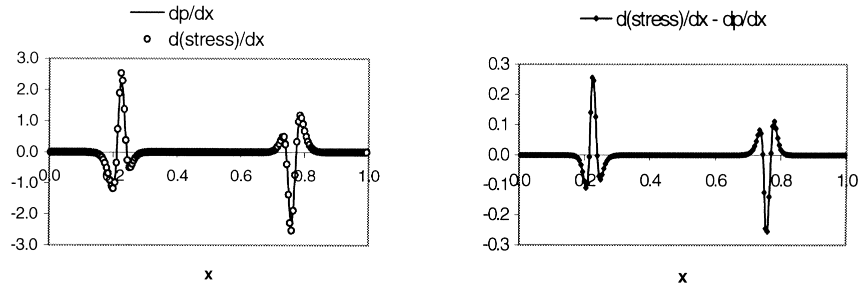

(a)

(b)

Fig. 7. Investigations of gradients of pressure and interfacial stress: (a) gradients of pressure and interfacial stress; (b) difference between the gradients of pressure and interfacial stress.

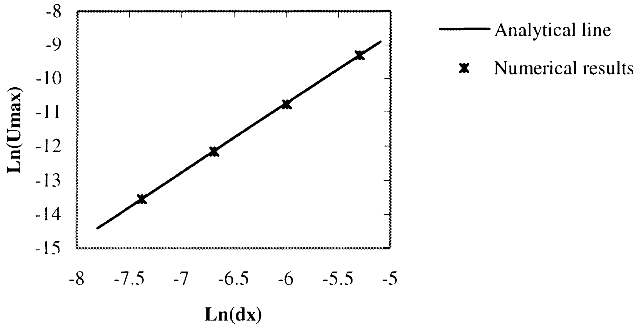

Fig. 8. Relation between the mesh spacing Δx and the maximum spurious velocity in the interface, plotted on a log-log scale. Here Δx is 1/200, 1/400, 1/800 and 1/1600, respectively.

4.2. Investigations of the interface

4.2.1. Density profile and interface thickness

To demonstrate how the density profile changes with different temperatures and surface tension, a planar interface is set up after the system is relaxed to non-dimensional time 100 when the two-phase fluid gets to equilibrium completely. The system size is 0.5 × 1.0 with a 50 × 100 computational grid. In order to show and compare different interfaces clearly, interfacial regions are cut from the whole systems to be shown in Fig. 4 and 5. Fig. 4 shows the shape of the equilibrated interface at different temperatures but under the same Weber number. With the decrease of the temperature, the density ratio and the surface tension increase and the interface becomes sharper and sharper. It is also seen that when the temperature approaches the critical point, the interface becomes smooth and the surface tension becomes smaller. The distinctions between the two phases will eventually vanish at the critical temperature. The density profile at the same T but different Weber number is also studied and results are shown in Fig. 5. From Eq. (2.14) we can see that there are two factors which can determine the surface tension, one is the reference Weber number which we can prescribe preliminarily and the other is density gradient which is related to T and the Weber number, respectively. Fig. 5 shows that with the increase of We_r, the surface tension is decreased because the increment of the density gradient caused by this operation is not as large as the effect of the decrement of the inverse of We_r. This figure also verifies that the density ratio is only determined by the temperature.

4.2.2. Discussions of the existence of spurious velocities

The equilibrium density, pressure (2.15), interfacial stress (2.13) profiles and the distribution of the spurious velocities normal to a flat interface are shown in Fig. 6(a)–(d). The simulation is carried out at $T = 0.9$ and $We_r = 40\,000$ with a 100×200 computational grid. The final time is $t = 400$ when all variables do not vary with time any more. From Fig. 6(a) and (b) we can see that distributions of pressure and interfacial stress profiles are about the same in equilibrium. In bulk phases, the pressure and interfacial stress are constants (zero for the interfacial stress). The existence of the spurious velocities is due to the errors of the discreteness of space and time inherent in the numerical simulations, which is experienced by both lattice Boltzmann and macroscopic finite-difference simulations. This can be analyzed from the momentum conservation Eq. (2.11) when the spurious velocities as shown are so small in equilibrium that the viscous stress tensor $\sigma^{(v)}$ in (2.11) could be neglected. Fig. 7(a) shows the gradients of the pressure and the interfacial stress, respectively. Fig. 7(b) provides a more transparent demonstration of their difference i.e. the right-hand side of (2.11). Then the reason for the spurious velocities' existence is clear. It is due to the unbalanced gradients of the pressure and the interfacial stress, which is caused by errors of finite difference schemes. As we know, the density profile must be monotonic with respect to the position, and then according to mass conservation Eq. (2.10), velocities everywhere in the system should be zero. This can also be further validated when a finer mesh and a smaller time step are used in the simulation so that the spurious velocities decrease as the discretization errors become smaller. For sufficiently fine grids, the discretization error is proportional to the leading term in the Taylor series (Ferziger and Peric, 1996):

$$\varepsilon_h^{\mathrm{d}} \approx ah^p + H,$$

where $\varepsilon_h^{\mathrm{d}}$ is the discretization error, h the mesh spacing, p the order of the scheme, H stands for higher order terms and a depends on the derivatives at the given point but is independent of h. Fig. 8 shows the relationship between the maximum spurious velocities and the mesh spacings of the system on a log-log plot when the same Courant number 0.01 is used. The slope of the analytical line is 2 since the scheme we used is second order accurate. This figure verifies that the spurious velocities are completely due to the discretization errors of the finite difference methods employed to solve the discrete Boltzmann equation.

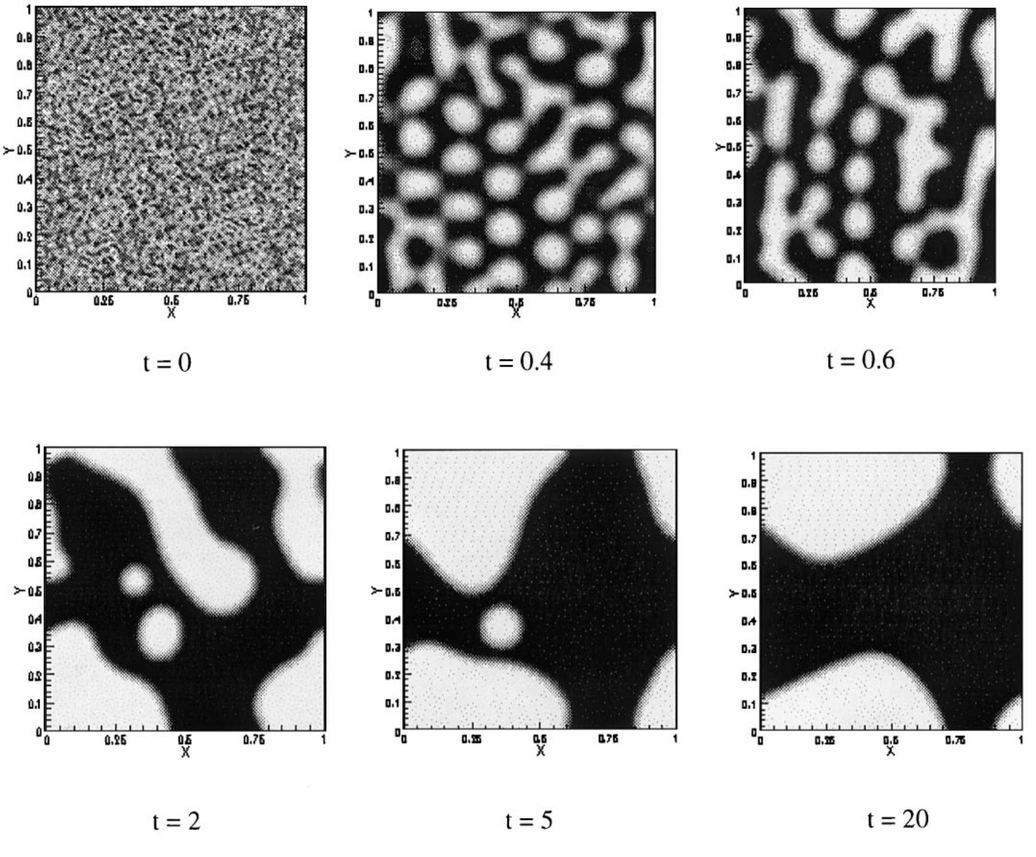

t = 0 t = 0.4 t = 0.6

t = 2 t = 5 t = 20

Fig. 9. Snapshots of two-dimensional phase separation at different times. Computational domain: 1×1 with a 100×100 computational mesh, $We_r = 10\,000$.

4.3. Phase separation

Here we demonstrate the phenomenon of phase separation both in two- and three-dimensional systems. The temperature is set as $T = 0.6$ corresponding to the density ratio of 40. When a homogenous vapor on or above the critical point is rapidly quenched to below the critical point where two or more different phases may coexist, the homogeneous vapor becomes unstable and a part of it should condense so that a liquid and a vapor phase coexist in equilibrium. In order for the liquid phase to be formed, it is necessary for the substance to condense on nuclei. These nuclei can be formed by ions or be presented in the form of dust or other small particles. Once the substance begins to condense on nuclei, the vapor–liquid equilibrium is rapidly established. This phenomenon is also called the spinodal decomposition and is of both theoretical interest and practical value (Osborn et al, 1995; Appert et al., 1995). In our numerical simulations, we give a random noise of amplitude 0.1 ρ_c representing the nuclei in the density field, which is superposed over an average density of ρ_c as the initial condition. The system is then quenched from the critical point to the state of 0.6 T_c. Snapshots of phase separation at different times are shown in Fig. 9 for two-dimensional system and Fig. 10 for three-dimensional system. Simulation parameters are given in the captions to the figures. From these two figures we can see that after the temperature quench, a part of the vapor rapidly condensed on 'nuclei', and the average size of the coexisting phases' domains tends to increase in an effort to decrease the interfacial energy. Finally two bulk coexisting phases formed in equilibrium. Some detailed investigations such as the rate of growth of the average size of these domains need to be studied later.

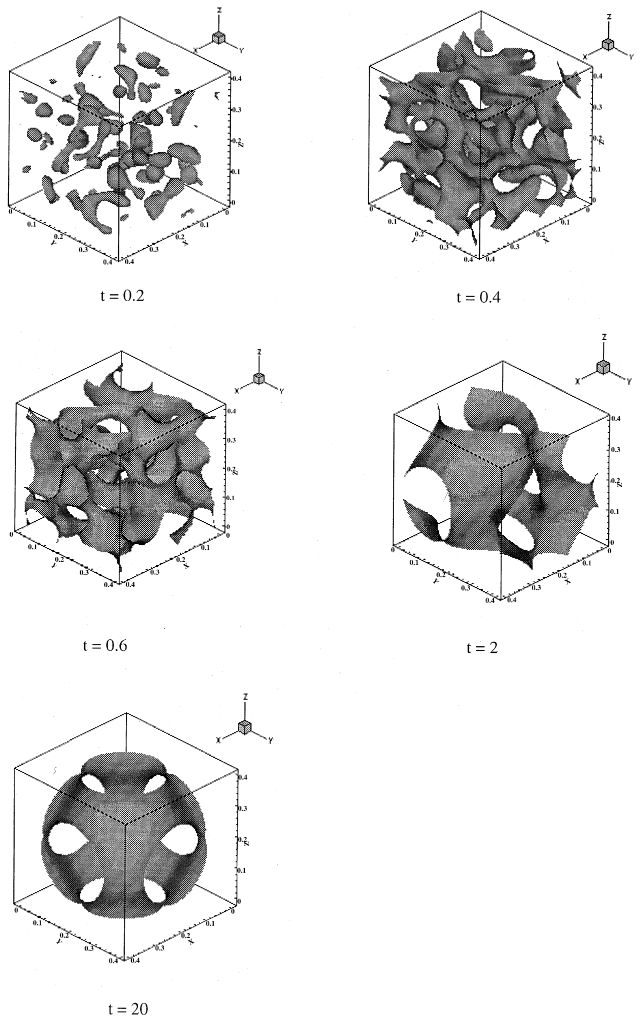
t = 0.2

t = 0.4

t = 0.6

t = 2

t = 20

Fig. 10. Snapshots of three-dimensional phase separation at different times. Computational domain: $0.4 \times 0.4 \times 0.4$ with a $40 \times 40 \times 40$ computational mesh, $We_r = 20000$.

5. Conclusions

In this paper, we have employed the TVD/AC scheme to the lattice Boltzmann multiphase model. Unlike the conventional CFD methods (Brackbill et al., 1992; Chang et al., 1996), the LBM does not need to track the position or calculate the curvature of interfaces. The phase transition and interfacial dynamics, which are essential for multiphase flows but difficult to handle at the macroscopic level, can be modeled naturally through the LBM by incorporating intermolecular interaction. Our approach also overcomes the common shortcomings of the traditional LBM. We provide a new simulator which is much helpful in stabilizing the computation in the runs of high-density ratios to solve the traditional lattice Boltzmann equation and makes it a more prospective method both in theoretical studies and engineering applications of the multiphase flows.

Numerical results for the coexistence curve are shown to be in excellent agreement with the analytic calculations over a very wide range of density ratios. Verification of Laplace law both in two and three dimensions shows the complete success of the TVD/AC scheme in lattice Boltzmann equation. The detailed dynamical behaviors of the interface such as interface thickness, the profiles of density, pressure and interfacial stress, the spurious velocities and so on are studied. Phase separation in two- and three-dimensional systems have also been numerically demonstrated. As for non-zero flows, we have used our approach to simulate phenomenon such as droplet deformation under shear flow and the results will be given elsewhere.

Further urgent challenges for the lattice Boltzmann method are some engineering applications. We hope this paper can make a useful step in this direction.

References

Alexander, F.J., Chen, S., Sterling, J.D., 1993. Lattice Boltzmann thermohydrodynamics. Phys. Rev. E 47, R2249–R2252.

Appert, C., Olson, J.F., Rothman, D.H., Zaleski, S., 1995. Phase separation in a three-dimensional, two-phase hydrodynamic lattice gas. J. Stat. Phys. 81, 181–197.

Benzi, R., Succi, S., Vergassola, M., 1992. The lattice Boltzmann-equation theory and applications. Phys. Rep. 222, 145–197.

Brackbill, J.U., Kothe, D.B., Zemach, C., 1992. A continuum method for modeling surface tension. J. Comp. Phys. 100, 335–354.

Chang, Y.C., Hou, T.Y., Merriman, B., Osher, S., 1996. A level set formulation of Eulerian interface capturing methods for incompressible fluid flows. J. Comp. Phys. 124, 449–464.

Chen, H., Chen, S., Matthaeus, W.H., 1991. Recovery of the Navier–Stokes equations using a lattice gas Boltzmann method. Phys. Rev. A 45, R5339–R5342.

Chen, S., Doolen, G., 1998. Lattice Boltzmann method for fluid flows. Annu. Rev. Fluid Mech. 30, 329–364.

Chen, Y., Teng, S., Shukuwa, T., Ohashi, H., 1998. Lattice Boltzmann simulation of two-phase fluid flows. Int. J. Mod. Phys. C 9, 1383–1391.

Ferziger, J.H., Peric, M., 1996. Computational Methods for Fluid Dynamics. Springer Press, Germany, pp. 58–66.

Frisch, U., d'Humières, D., Hasslacher, B., Lallemand, P., Pomeau, Y., River, J.P., 1987. Lattice gas hydrodynamics in two and three dimensions. Complex Syst. 1, 649–707.

Grunau, D., Chen, S., Eggert, K., 1993. A lattice Boltzmann model for multiphase fluid flows. Phys. Fluids A 5, 2557–2562.

Gunstensen, A.K., Rothman, D.H., Zaleski, S., Zanetti, G., 1991. Lattice Boltzmann model of immiscible fluids. Phys. Rev. A 43, 4320–4327.

Harten, A., 1983. High resolution schemes for hyperbolic conservation laws. J. Comp. Phys. 49, 357–393.

Hirschfelder, J.O., Curtiss, C.F., Bird, R.B., 1964. Molecular Theory of Gases and Liquids. Wiley, New York, pp. 250–262.

Jin, B., 1993. An artificial compression method for the computation of contact discontinuities. Comput. Math. (China) 1, 121–128.

Nadiga, B.T., Zaleski, S., 1996. Investigations of a two-phase fluid model. Eur. J. Mech. B/Fluids 15, 885–896.

Osborn, W.R., Orlandini, E., Swift, M.R., Yeomans, J.M., Banavar, J.R., 1995. Lattice Boltzmann study of hydrodynamic spinodal decomposition. Phys. Rev. Lett. 75, 4031–4034.

Press, W.H., Flannery, B.P., Teukolsky, S.A., Vetterling, W.T., 1989. Numerical Recipes. Cambridge University Press, Cambridge, pp. 551–554.

Qian, Y.H., d'Humières, D., Lallemand, P., 1992. Lattice BGK Models for Navier-Stokes Equation. Europhys. Lett. 17, 479–484.

Qian, Y.H., Succi, S., Orszag, S.A., 1995. Recent advances in lattice Boltzmann computing. Annu. Rev. Comp. Phys. 3, 195–242.

Rothman, D.H., Keller, J.M., 1988. Immiscible cellular-automaton fluids. J. Stat. Phys. 52, 1119–1127.

Rowlinson, J.S., Widom, B., 1982. Molecular Theory of Capillarity. Clarendon Press, Oxford, pp. 26–56.

Shan, X., Chen, H., 1993. Lattice Boltzmann model for simulating flows with multiphase and components. Phys. Rev. E 47, 1815–1819.

Shan, X., Chen, H., 1994. Simulation of nonideal gases and liquid-gas phase transitions by the lattice Boltzmann equation. Phys. Rev. E 49, 2941–2948.

Shan, X., Doolen, G., 1995. Multicomponent lattice-Boltzmann model with interparticle interaction. J. Stat. Phys. 81, 379–394.

Swift, M.R., Osborn, W.R., Yeomans, J.M., 1995. Lattice Boltzmann simulation of non-ideal fluids. Phys. Rev. Lett. 75, 830–833.

Swift, M.R., Orlandini, E., Osborn, W.R., Yeomans, J.M., 1996. Lattice Boltzmann simulations of liquid-gas and binary fluid systems. Phys. Rev. E 54, 5041–5052.

Zou, Q., He, X., 1999. Derivation of the macroscopic continuum equations for multiphase flow. Phys. Rev. E 59, 1253–1255.